# letters

# DNA binding is required for the apoptogenic action of apoptosis inducing factor

Hong Ye[1], Celine Cande[2], Nicolas C. Stephanou[1], Sulin Jiang[1], Sundeep Gurbuxani[3], Nathanael Larochette[2], Eric Daugas[2], Carmen Garrido[3], Guido Kroemer[2] and Hao Wu[1]

[1]Department of Biochemistry, Weill Medical College of Cornell University, 1300 York Avenue, New York, New York 10021, USA. [2]Centre National de la Recherche Scientifique, UMR1599, Institut Gustave Roussy, 39 rue Camille Desmoulins, F-94805 Villejuif, France. [3]INSERM U-517, Faculty of Medicine and Pharmacy, 7 Boulevard Jeanne d'Arc, 21033 Dijon, France.

**The execution of apoptosis or programmed cell death comprises both caspase-dependent and caspase-independent processes. Apoptosis inducing factor (AIF) was identified as a major player in caspase-independent cell death. It induces chromatin condensation and initial DNA cleavage *via* an unknown molecular mechanism. Here we report the crystal structure of human AIF at 1.8 Å resolution. The structure reveals the presence of a strong positive electrostatic potential at the AIF surface, although the calculated isoelectric point for the entire protein is neutral. We show that recombinant AIF interacts with DNA in a sequence-independent manner. In addition, in cells treated with an apoptotic stimulus, endogenous AIF becomes co-localized with DNA at an early stage of nuclear morphological changes. Structure-based mutagenesis shows that DNA-binding defective mutants of AIF fail to induce cell death while retaining nuclear translocation. The potential DNA-binding site identified from mutagenesis also coincides with computational docking of a DNA duplex. These observations suggest that AIF-induced nuclear apoptosis requires a direct interaction with DNA.**

Apoptosis is a highly organized multi-step process, with the induction of mitochondrial membrane permeabilization as a decisive event in the commitment to cell death[1,2]. Apoptosis inducing factor (AIF), a resident protein of the inter-mitochondrial space, has been implicated as a crucial early effector of apoptosis[3], acting before or in parallel with the onset of caspase-dependent processes[4]. Genetic knockout of AIF abolishes the first wave of apoptosis that is indispensable for early embryonic morphogenesis[5]. In contrast, the ectopic presence of AIF in the extra-mitochondrial compartment suffices to kill cells[3]. When released from the mitochondria or added to purified nuclei, AIF enters the nucleus and induces chromatin condensation and large-scale DNA fragmentation to ~50 kilobases (kb) in a caspase-independent fashion[3,6]. The apoptogenic properties of AIF are conserved throughout evolution, from the facultative multicellular organism *Dictiostelium discoideum* to mammals[7].

Human AIF is synthesized as a precursor protein of 67 kDa and converted to mature AIF of 57 kDa upon mitochondrial import and removal of the N-terminal mitochondrial localization signal[3]. Mature AIF is a flavoprotein with weak but significant sequence similarity to bacterial nicotinamide adenine dinucleotide (NAD)-dependent oxidoreductases, suggesting that AIF is a bifunctional protein with a mitochondrial resident function and an apoptogenic function. Because the flavin adenine dinucleotide (FAD) cofactor is dispensable for the apoptogenic function but required for the oxidoreductase activity of AIF[3,8], the structural bases for the mitochondrial and ectopic functions of AIF are probably entirely different. To understand the molecular mechanism of AIF-induced apoptosis, we determined the crystal structure of mature human AIF at 1.8 Å resolution (Fig. 1a,b). The structure is highly similar to that of the mature mouse AIF[9].
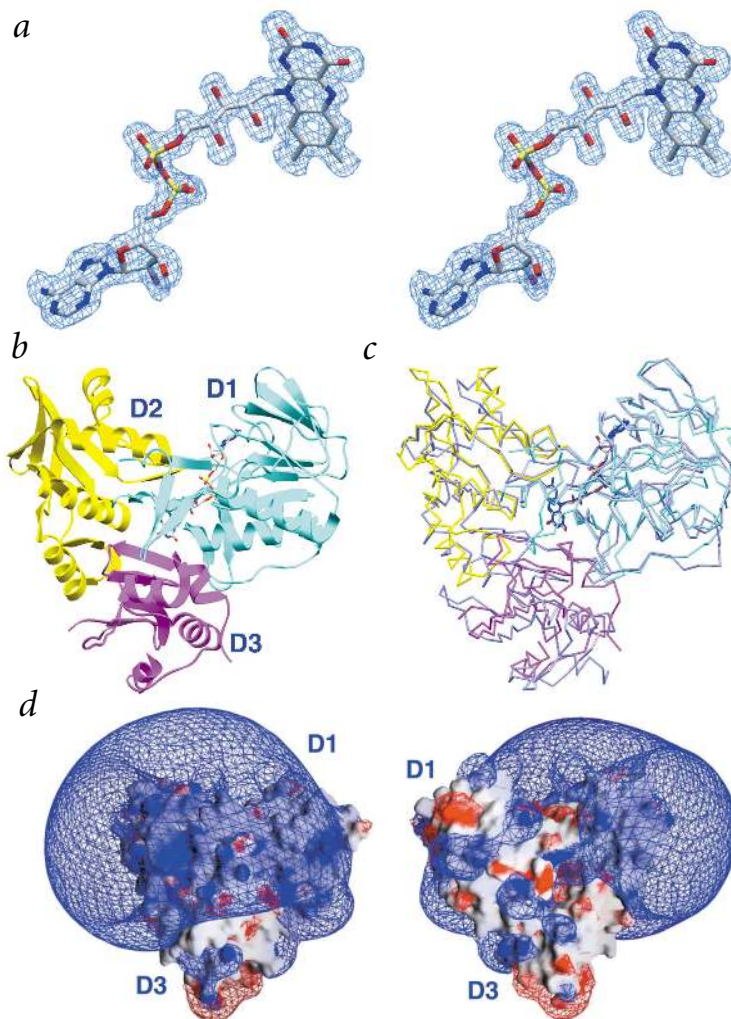


**Fig. 1** Structure of AIF. *a*, Stereo view of the $2F_o - F_c$ electron density and the superimposed FAD cofactor of AIF, shown at 1.0 σ contour. *b*, Ribbon diagram of the structure, showing the three domains (D1 in cyan, D2 in yellow and D3 in magenta). *c*, Superposition of AIF and BphA4 (BphA4 in light blue). The FAD cofactor is shown in stick models (atomic colors for AIF and dark blue for BphA4). *d*, Electrostatic potential of AIF (left and right panels are related by 180° rotation along the vertical axis). The surface and the contour are colored from $-10 k_b T e^{-1}$ (red) to $10 k_b T e^{-1}$ (blue) and from $-1.5 k_b T e^{-1}$ (red) to $1.5 k_b T e^{-1}$ (blue), respectively, where $k_b$, T and e are the Boltzmann constant, temperature and the electron charge, respectively .
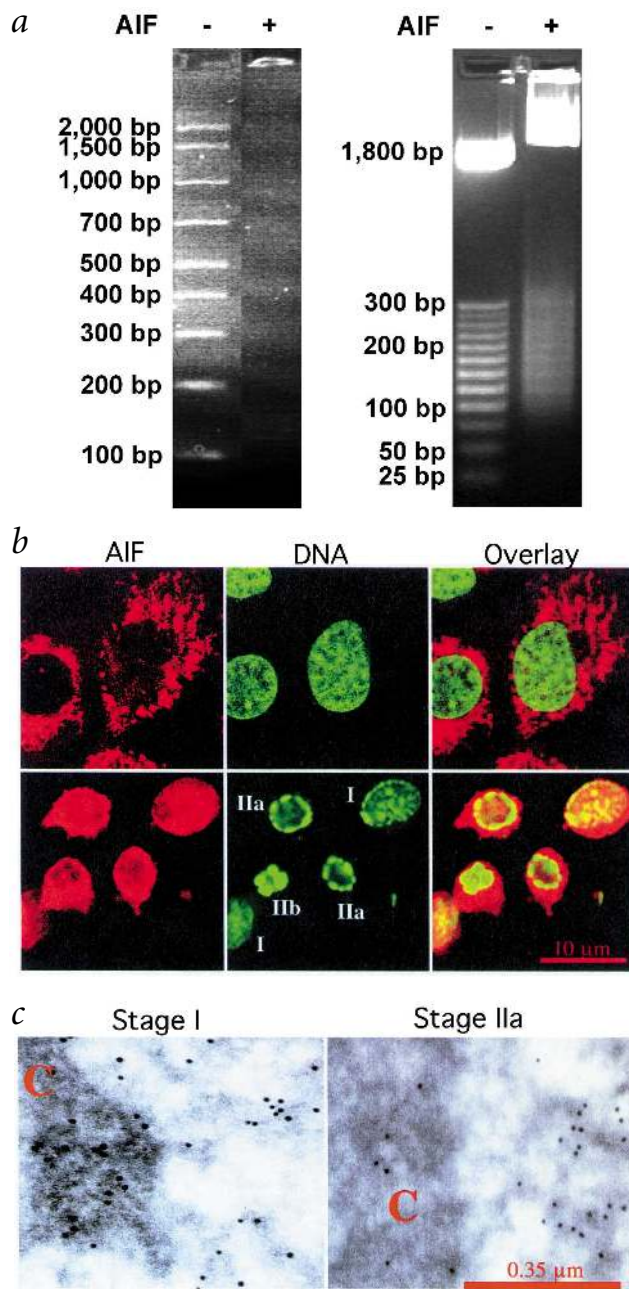
**Fig. 2** AIF interacts and co-localizes with DNA. *a*, The retardation of DNA migration by AIF on 3% agarose gels. In the left panel, the quantity of AIF used completely prevents the migration of the DNA fragments (100–2,000 bp), as shown by DNA staining in the well. In the right panel, DNA retardation is observed for the interaction of AIF with DNA fragments as short as 25 bp, as shown by the disappearance of the DNA fragments at their normal migration positions and the smearing of the DNA staining in the presence of AIF. The lower ratio of AIF to DNA in the right panel results in smearing rather than complete prevention of migration. *b*, Co-localization of AIF with DNA during stage I of chromatin condensation. Rat-1 cells, untreated (upper panel) or cultured with 2 µM staurosporin for 4 h (lower panel) were fixed and immunostained[29] for the detection of AIF (red) and DNA (SYTOX Green, Molecular Probes). *c*, Staurosporin-treated Rat-1 cells, subjected to ultrathin sectioning, uranylacetate-oxalate counterstaining and immunogold diction of AIF (5 nm particles). C refers to compact areas of chromatin condensation.

domain movements. In addition, the D3 domain of AIF contains a large insertion, part of which is disordered in the structure. The D1 and D2 domains appear to contain all the enzymatic functionalities for catalysis, because some similar oxidoreductases, such as the adrenodoxin reductase in the mitochondrial cytochrome P450 system, do not contain a D3 domain[12].

Despite having a calculated neutral isoelectric point (6.5 for mature human AIF), the surface of AIF possesses a striking positive electrostatic potential, which covers a large part of the AIF surface (Fig. 1*d*). This feature is not conserved in BphA4, which, conversely, has a more prominent negative electrostatic potential, suggesting that this feature of AIF is not important for the oxidoreductase function. The highest positive electrostatic potential centers at a convex surface of the D2 domain and extends to D1 and D3.

## Interaction and co-localization with DNA

The surface feature of AIF and the established effect of AIF on nuclear morphology and integrity suggest that AIF may interact with DNA directly and that such an interaction may be crucial for AIF function. Many DNA-binding proteins, such as the sliding clamp structure of the β-subunit of *E. coli* DNA polymerase III[13], as well as histones[14], show strong positive surface electrostatic potential. Accordingly, purified recombinant AIF interacted with DNA of different lengths, as shown by the gel retardation of every fragment in a 100 bp DNA ladder (100–2,000 base pairs (bp), and DNA as short as 25 bp (Fig. 2*a*). Because the DNA species in the experiment have different sequences and nucleotide compositions, these data indicate that AIF interacts with DNA in a sequence-independent manner. In contrast, AIF failed to interact with various single-stranded oligonucleotides.

We tested whether endogenous AIF co-localizes with DNA upon introduction of an apoptotic stimulus. We treated Rat-1 cells with 2 µM staurosporin for 4 h to induce mitochondrial membrane permeabilization. The cells were then fixed and stained with SYTOX Green for DNA and with an anti-AIF antibody[3,29] suitable for the detection of endogenous AIF (Fig. 2*b*). In nontreated cells, AIF clearly localized to the cytoplasm with a punctate distribution characteristic of mitochondrial proteins, and the chromatin remained unlabeled. In contrast, AIF in treated cells migrated to the nucleus and partially co-localized with areas of condensed chromatin during early apoptosis (stage I). Later, when DNA degraded to small oligonucleosomal DNA fragments (stage II), this co-localization of AIF and chromatin diminished. These observations were confirmed at the ultrastructural level, by immunogold detection of AIF in cells proceeding from an early stage of chromatin condensation (stage I) to chromatinolysis with formation of apoptotic bodies (stage II)

## AIF structure and the positive electrostatic potential

Structural alignment using the DALI server[10] revealed that, besides mouse AIF, human AIF is also structurally homologous to BphA4 (Fig. 1*c*), a bacterial oxygenase-coupled NADH-dependent ferredoxin reductase (ONFR) that has a fold similar to enzymes of the eukaryotic glutathione reductase family[11]. Based on the homology with BphA4, the structure of AIF may be divided into three domains, an FAD-binding domain (D1, residues 128–262 and 401–480), a putative NADH-binding domain (D2, residues 263–400) and a C-terminal domain (D3, residues 481–608). A structural alignment with a 3.0 Å Cα distance cutoff showed that almost all superimposable residues are located in the D1 and D2 domain, whereas the D3 domain of AIF is rather different from BphA4. Separate structural alignment using the D3 domain alone did not significantly improve the alignment, confirming that the poor alignment is not due to

# letters

**Fig. 3** Mutational analysis of AIF. *a*, Gel retardation by wild type and mutant AIF. Right panel was performed with higher quantities of AIF. *b*, Mapping of DNA-binding defective mutants onto AIF surface (light yellow). Left shows the groove between D1 and D3; middle, the same view with docked DNA duplex; and right, rotated 90° along the vertical axis to show the remaining patches on D3. Surface mutation clusters are colored cyan for m446 (Lys 446, Arg 449, Arg 450 and Arg 451 are labeled in red), green for m255 (Lys 255 and Arg 265 are labeled in blue), red for m584 (Arg 584, Lys 590 and Lys 593 are labeled in blue) and purple for m510 (Lys 510 and Lys 518 are labeled in red). *c*, Immunofluorescent images of mature AIF–GFP transfected cells, showing GFP alone, wild type AIF, m255, m510 and m192. Arrows show condensed chromatin indicative of apoptotic cell death.
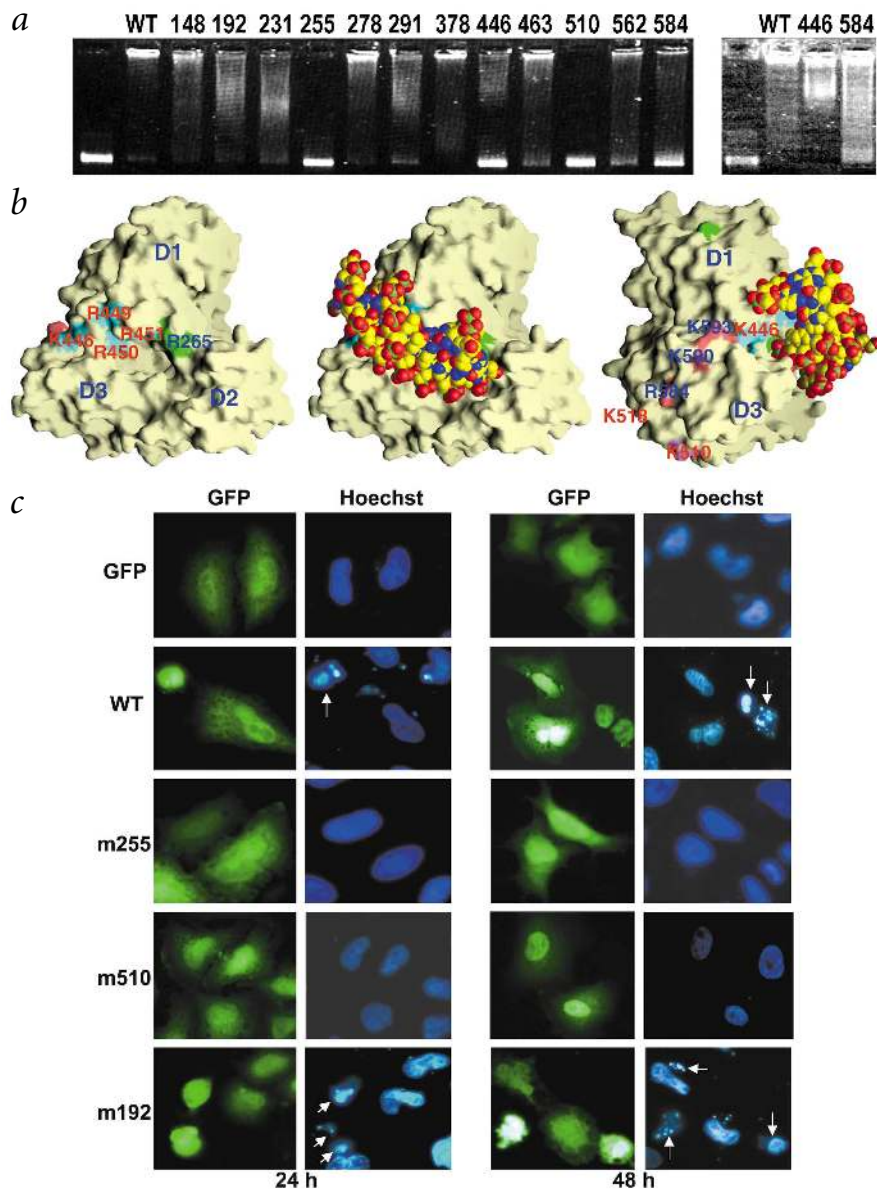


(Fig. 2*c*). The preferential association of AIF with chromatin during stage I of chromatin condensation is in accordance with its role as an early nuclear effector of apoptosis.

## DNA binding is required for apoptosis

To determine whether the DNA-binding activity of AIF correlates with its ability to induce apoptosis, we identified clusters of exposed positively charged residues along the AIF sequence and generated mutants with multiple Ala substitutions at the corresponding positions (Table 1). The mutations did not have drastic effects on the overall calculated electrostatic potential of AIF. However, gel retardation assays showed that several mutants, including m255, m446, m510 and m584, showed reduced affinity with DNA (Fig. 3*a*; Table 1). Although m255 and m510 failed to interact with DNA completely, m446 and m584 did cause DNA retardation at higher AIF concentrations, with m446 showing relatively stronger affinity to DNA than m584.

Mapping of all mutated positions in m255, m446, m510 and m584 — a total of 10 sites (Table 1; Fig. 3*b*) — onto the surface of AIF indicate that they form a continuous stretch that could form a potential DNA-interacting surface (with the exception of residue Lys 255 in the m255 mutant). This surface begins from the groove between D1 and D3 and extends to one face of the D3 domain. The location of these residues may provide an explanation for the function of the unique D3 domain in AIF. In agreement with this observation, a C-terminal deletion mutant of AIF failed to induce apoptosis (data not shown). Remarkably, computational docking of a DNA duplex (12 bp) onto the AIF surface showed that the DNA structure forms a low energy complex along the groove between D1 and D3 of AIF, suggesting that this may be an important DNA interaction site (Fig. 3*b*). The actual interaction between AIF and DNA may involve DNA longer than 12 bp, which could wrap around the AIF surface to reach the remaining DNA-interacting residues on the D3 domain. Such an interaction would require significant changes in standard DNA

duplex structure. Interestingly, the most positively charged convex D2 domain surface does not seem to be important for DNA interaction, suggesting that the interaction of AIF with DNA is not purely a nonspecific charge–charge attraction.

The ability of these AIF mutants to translocate to the nucleus and induce cell death was determined by transfection with mature AIF–GFP fusion constructs (Table 1; Fig. 3*c*). Although most AIF mutants showed comparable or delayed translocation into the nucleus at 24 h post transfection, suggesting that the surface positive charges in wild type AIF may be collectively involved in the nuclear localization, mutant m192 showed greatly accelerated nuclear translocation. However, complete translocation was achieved for all AIF mutants 48 h post transfection.

The cell death induction of AIF mutants was determined 48 h post-transfection when nuclear translocation was complete (Table 1; Fig. 3*c*). AIF mutants m255 and m510, which failed to interact with DNA *in vitro*, were completely unable to induce cell death. Mutants m446 and m584, which show weakened DNA interaction, also induced significantly or modestly lower levels of cell death. In contrast, AIF mutants that still interacted with

### Table 1 Apoptogenic and DNA-binding activity of wild type and mutant AIF[1]

| AIF | Nuclear translocation at 24 h (%) | Nuclear translocation at 48 h (%) | Cell death at 48 h (%) | DNA binding[2] |
|---|---|---|---|---|
| GFP | 2 | 9 | 5 ± 2 | – |
| AIF–GFP WT | 10 | >95 | 43 ± 3 | +++ |
| m148 | 2 | >95 | 30 ± 4 | +++ |
| m192 | 50 | >95 | 62 ± 2 | +++ |
| m231 | 10 | >95 | 53 ± 4 | +++ |
| m255 | 2 | >95 | 3 ± 3 | – |
| m278 | 9 | >95 | 41 ± 4 | +++ |
| m291 | 12 | >95 | 47 ± 3 | +++ |
| m446 | 2 | >95 | 38 ± 3 | ++ |
| m463 | 2 | >95 | 43 ± 3 | +++ |
| m510 | 27 | >95 | 2 ± 2 | – |
| m562 | 10 | >95 | 41 ± 5 | +++ |
| m584 | 2 | >95 | 26 ± 5 | + |

[1]Mutant abbreviations are as follows: m148 contains R148A, R151A, R153A, R158A; m192: R192A, K194A; m231: K231A, K232A, R239A, K244A; m255: K255A, R265A; m278: K278A, R280A, R285A, K286A; m291: R291A, K295A, R298A, K301A; m446: K446A, R449A, R450A, R451A; m463: R463A, K474A; m510: K510A, K518A; m562: K562A, R569A, K571A; and m584: R584A, K590A, K593A.
[2]DNA binding is scored based on the quantity of AIF needed to retard DNA migration. DNA retardation at lower AIF quantity, +++ (Fig. 3a, left panel); complete and partial DNA retardation, ++ and +, respectively, at higher AIF quantity (Fig. 3a, right panel); and no DNA retardation at either lower or higher AIF quantity, –.

DNA retained the ability to induce cell death similar to the wild type AIF. The level of cell death induction seems to be modulated by the rate of nuclear localization, because the m192 mutant, which showed enhanced nuclear translocation, was significantly more effective in inducing cell death. The nature of cell death induction by wild type and mutant AIF is apoptotic, as shown by chromatin condensation (Fig. 3c). These observations demonstrate that the apoptogenic activity of AIF requires direct interaction with DNA, which may be further modulated by the rate of nuclear translocation. None of the AIF mutations resulted in disruption of protein integrity or dramatic changes in the redox activity.

## Discussion

How does the binding of AIF to DNA induce chromatin condensation? We hypothesize that the interaction of AIF with DNA may reconfigure DNA or chromatin structure. Although organized chromatin condensation during mitosis is an ATP-dependent process that requires large molecular machines[15], chromatin condensation during apoptosis is probably a more passive event. By interacting directly with DNA and possibly displacing chromatin-associated proteins, AIF could disrupt normal chromatin structure, leading to a 'collapse' of DNA and the appearance of condensation. The function of AIF on DNA integrity may be similarly exerted because chromatin remodeling upon AIF interaction may increase the susceptibility of DNA to nucleases. Alternatively, AIF may recruit downstream nucleases to induce caspase-independent partial chromatinolysis, because AIF itself is devoid of any nuclease activity[3,6]. The characteristic size distribution of DNA fragments in AIF-treated cells corresponds to higher order chromatin structures known as loop domains[16,17]. As topoisomerase II or cyclophilins can induce the generation of similar ~50 kb DNA fragments from nuclear DNA[18,19], these may represent potential downstream effectors of

AIF. In summary, irrespective of the exact mechanisms through which AIF induces chromatin condensation and chromatinolysis, it appears clear that its interaction with DNA is essential for this function.

## Methods

**Protein expression, purification and crystallization.** Human mature AIF (residues 121–613) was overexpressed in *E. coli* with overnight IPTG induction, 0.5 mM IPTG at 20 °C. The protein contains both N- and C-terminal His-tags and was purified by Ni-affinity chromatography and gel filtration. The protein was then concentrated to 6 mg ml^{-1} and crystallized under 16% (w/v) PEG 8000 and 5 mM dithiothreitol (DTT) in 100 mM Tris, pH 8.0. For phase determination, selenomethionyl AIF was produced and crystallized similarly.

**Structure determination.** Preliminary crystal characterization was conducted on Raxis-IV imaging plate detectors mounted on Rigaku RU300 X-ray generators. Although most of the crystals are in the C2 space group, the best diffracting ones belong to the P2$_1$ space group. SAD data from a selenomethionyl AIF crystal in the P2$_1$ space group were collected to 1.9 Å resolution at the selenium peak (wavelength 0.9793 Å) at the ID19 beamline of SBC-CAT of the advanced photon source. They were processed and scaled with HKL2000[20]. SAD phasing was performed with SOLVE[21] and ~80% of the structure was auto-built with ARP/wARP[22]. Structural refinement was performed with the simulated annealing protocol in CNS[23] against a native diffraction data set in the P2$_1$ space group at 1.8 Å resolution. Manual model manipulations were carried out in O[24]. The current atomic model of AIF contains residues 128–182, 185–539 and 560–608, with two disordered internal stretches and disordered N- and C-terminal tails. Crystallographic statistics are shown in Table 2. Ribbon and stick models were created using

### Table 2 Crystallographic statistics[1]

| Data collection | |
|---|---|
| Space group | P2$_1$ |
| Unit cell | |
| a (Å) | 50.9 |
| b (Å) | 90.5 |
| c (Å) | 60.5 |
| β (°) | 94.6 |
| Resolution (Å) | 40–1.9 |
| R$_{sym}$ (%)[2] | 5.9 (25.8) |
| Completeness (%)[2] | 99.1 (98.0) |
| SOLVE[3] score | 48.6 |
| Figure of merit | 0.41 |
| | |
| **Refinement** | |
| Resolution (Å) | 40–1.8 |
| R$_{sym}$ (%)[2] | 6.2 (26.4) |
| Completeness (%)[2] | 99.4 (99.6) |
| Number of reflections | 44,620 |
| Number of atoms | |
| Protein | 3,579 |
| Solvent | 235 |
| R-factor (%) | 22.5 |
| R$_{free}$ (%) | 24.2 |
| R.m.s deviation | |
| Bond lengths (Å) | 0.006 |
| Bond angles (°) | 1.3 |
| Bond B-factor (Å$^2$) | 2.5 |
| Ramachandran analysis | 99.3% in allowed regions |

[1]Phase determination by single-wavelength anomalous diffraction (SAD) from a selenomethionyl crystal at λ = 0.9793 Å.
[2]Numbers in parentheses are for the last shell.
[3]Ref. 21.

# letters

SETOR[25], and molecular surface representations were calculated and presented by GRASP[26].

**Gel retardation assays.** The interaction of wild type AIF with DNA molecular weight ladders was performed by gel retardation on 3% agarose gels pre-stained with ethidium bromide. A 5 μl sample of the 50 bp DNA ladder (50–2,000 bp at 100 ng μl⁻¹, 50 bp fragment not easily visible; BioRad) and a 4 μl sample of the 25 bp DNA ladder (25–300 bp plus 1,800 bp at 360 ng μl⁻¹; Promega) were incubated with 5 μl and 10 μl AIF (5 μg μl⁻¹), respectively, for 30 min at room temperature before electrophoresis.

The interaction of wild type and mutant AIF with DNA was carried out by gel retardation on 1% agarose gels. Wild type and mutant AIF (8 μl or 12 μl at 0.8 μg μl⁻¹) were incubated with 1 μl of a 1,500 bp DNA fragment (20 ng μl⁻¹) for 30 min at room temperature, electrophoresed and stained with nucleic acid dye SYBR Green I (Sigma).

**Docking calculations.** A 12 bp DNA duplex structure (PDB accession 1FQ2) was docked onto the surface of AIF using GRAMM[27], which uses a surface complementarity algorithm to identify contact regions between macromolecular partners. A calculation at 1.9 Å resolution indicated a strong preference of the DNA duplex for the surface groove between D1 and D3, onto which numerous DNA-binding defective mutations are mapped. Specifically, 6 of the 10 lowest energy complexes obtained from GRAMM formed a tight cluster at this binding site of AIF, whereas the other four complexes were scattered. Such clustering is a strong indication of the real binding site.

**Apoptogenic assay.** Nonconfluent mouse embryonic fibroblasts (seeded 1 d before transfection at $2.0 \times 10^4$ cells per well) were transfected with the indicated mature AIF–GFP constructs (0.6 μg of DNA per well), using the SuperFect Transfection reagent (Qiagen), in a Lab-Tek chamber slide system (Nalge Nunc International). At different intervals (24 and 48 h), the percentage of cells showing nuclear enrichment of GFP-dependent fluorescence was assessed by immunofluorescence microscopy as described[28]. Chromatin condensation was detected by staining with Hoechst 33342 (Sigma)[29]. Cell death, as assessed by loss of adherence, was determined using the crystal violet assay at 48 h (ref. 30). Results are mean values of triplicate measurements ± s.d.

**Redox activity assay.** The kinetic parameters for the redox activity were measured as described[8] by varying NADH concentration (10 μM–4 mM) in the presence of 1.3 mM 2,2′-di-*p*-nitrophenyl-5-5′-diphenyl-3,3′[3-3′-dimethoxy-4-4′diphenylene]ditetrazolium chloride (NBT) in 250 μM MES, pH 5.5. Optical absorbance measurements at 560 nm were performed on a MRX Dynex UV-visible spectrophotometer.

**Coordinates.** The atomic coordinates have been deposited in the Protein Data Bank (accession code 1M6I).

1. Zamzami, N. & Kroemer, G. *Nature Rev. Mol. Cell Biol.* **2**, 67–71 (2001).
2. Wang, X. *Genes Dev.* **15**, 2922–2933 (2001).
3. Susin, S.A. *et al. Nature* **397**, 441–446 (1999).
4. Green, D.R. *Cell* **94**, 695–698 (1998).
5. Joza, N. *et al. Nature* **410**, 549–554 (2001).
6. Susin, S.A. *et al. J. Exp. Med.* **192**, 571–580 (2000).
7. Arnoult, D. *et al. Mol. Biol. Cell* **12**, 3016–3030 (2001).
8. Miramar, M.D. *et al. J. Biol. Chem.* **276**, 16391–16398 (2001).
9. Mate, M.J. *et al. Nature Struct. Biol.* **9**, 442–446 (2002).
10. Holm, L. & Sander, C. *Trends Biochem. Sci.* **20**, 478–480 (1995).
11. Senda, T. *et al. J. Mol. Biol.* **304**, 397–410 (2000).
12. Ziegler, G.A., Vonrhein, C., Hanukoglu, I. & Schulz, G.E. *J. Mol. Biol.* **289**, 981–990 (1999).
13. Kong, X.P., Onrust, R., O'Donnell, M. & Kuriyan, J. *Cell* **69**, 425–437 (1992).
14. Luger, K., Mader, A.W., Richmond, R.K., Sargent, D.F. & Richmond, T.J. *Nature* **389**, 251–260 (1997).
15. Uhlmann, F. *Curr. Biol.* **11**, R384–387 (2001).
16. Demeret, C., Vassetzky, Y. & Mechali, M. *Oncogene* **20**, 3086–3093 (2001).
17. Benbow, R.M. *Science Prog.* **76**, 425–450 (1992).
18. Li, T.K. *et al. Genes Dev.* **13**, 1553–1560 (1999).
19. Montague, J.W., Hughes, F.M. Jr & Cidlowski, J.A. *J. Biol. Chem.* **272**, 6677–6684 (1997).
20. Otwinowski, Z. & Minor, W. *Methods Enzymol.* **276**, 307–326 (1997).
21. Terwilliger, T.C. & Berendzen, J. *Acta Crystallogr. D* **55**, 849–861 (1999).
22. Perrakis, A., Morris, R. & Lamzin, V.S. *Nature Struct. Biol.* **6**, 458–463 (1999).
23. Brünger, A.T. *et al. Acta Crystallogr. D* **54**, 905–921 (1998).
24. Jones, T.A., Zou, J.-Y., Cowan, S.W. & Kjeldgaard, M. *Acta Crystallogr. A* **47**, 110–119 (1991).
25. Evans, S.V. *J. Mol. Graph.* **11**, 134–138 (1993).
26. Nicholls, A., Sharp, K.A. & Honig, B. *Proteins* **11**, 281–296 (1991).
27. Katchalski-Katzir, E. *et al. Proc. Natl. Acad. Sci. USA* **89**, 2195–2199 (1992).
28. Loeffler, M. *et al. FASEB J.* **15**, 758–767 (2001).
29. Daugas, E. *et al. FASEB J.* **14**, 729–739 (2000).
30. Ravagnan, L. *et al. Nature Cell Biol.* **3**, 839–843 (2001).